Hydrodynamic model development for the Trinity River Delta

Zhi Li, M.S.
Paola Passalacqua, Ph.D.
Ben R. Hodges, Ph.D.

submitted by
Center for Water and the Environment
The University of Texas at Austin

Submitted to the Texas Water Development Board
Final report under contract no. 1600011928
July 19, 2018

Executive Summary

A hydrodynamic model (the newly-written Frehd-C) has been constructed to investigate mismatch of flow between different measurement locations across the Trinity Delta and provide the foundations for the Trinity Delta Hydrodynamic Model (TDHM). The model bathymetry is generated from lidar data with extensive analyses as described in this report. The available lidar data does not contain trustworthy values regarding the bottom elevation in submerged areas of the delta, so a limited ground-truth field survey was conducted. Two methods are used to separate the water regions and the land regions in the lidar data such that estimated bottom elevations can be assigned to the water regions to maintain surface connectivity in the model. These methods are (i) an automatic clustering algorithm that identifies the water areas by their color from a GoogleEarth satellite image, and (ii) a manual delineating method that identifies additional channel connectivity in Photoshop. Two hydrodynamic simulations were executed with the bathymetries created by these two methods. Comparison between the two simulations shows different patterns regarding surface wave propagation and salinity transport because the automatic clustering algorithm fails to identify many narrow channels in the mid-to-upper delta. This comparison indicates the significant impact of the bathymetry processing on simulation results. The potential of Frehd-C in modeling the hydrodynamics of the Trinity Delta has been shown. However, for the model to be used to solve realistic problems will require (i) more bathymetry data for submerged regions than was collected in this project, (ii) analysis and processing of comprehensive boundary condition data for inflows, tidal elevation and winds, and (iii) an additional field data collection program throughout the delta for model calibration and validation. Finally, it should be noted that the Frehd-C model does not (at this time) include algorithms representing the slow, near-surface groundwater flows that are likely to affect water movement through the delta.

Contents

1 Introduction **3**

2 Lidar data processing **4**
2.1 Creating a Digital Elevation Model (DEM) from lidar data 4
2.2 Noise removal and water body identification 4

3 Validation with field survey measurements **10**

4 Preliminary development of TDHM **13**
4.1 Hydrodynamic model selection 13
4.2 Modeling scenarios 14
4.3 Model results 19

5 Summary and future tasks **24**

1 Introduction

Mismatch of river discharge between Romayor gage (08066500) and Wallisville gage (08067252) has been previously detected based on data collected by the U.S. Geological Survey (USGS). To improve understanding of the timing and spatial distribution of Trinity River water entering the Trinity Bay, a two-dimensional (2D) hydrodynamic model, the Trinity Delta Hydrodynamic Model (TDHM), is being developed to model transport and exchange through this region. Such models require extensive input data, including detailed bathymetry information, initial conditions for water surface elevations, and boundary conditions on flows and depths. This report summarizes the preliminary work required for model construction, which included three tasks:

1. Mobilizing lidar data and analysis of "not-a-number" (NaN) elements.
2. Field work for limited checking of NaN elements and bathymetry in some channels.
3. Analysis of landscape data and development of a hydrodynamic model.

Model bathymetry is created by upscaling (i.e., coarsening) lidar data to a grid resolution that is practical for hydrodynamic modeling. This task requires extensive analyses to ensure that data errors in the lidar data are not translated into the model bathymetry. The high-resolution lidar data of the Trinity Delta topography contains many NaN elements in regions containing deep channels and lakes because the red laser light used in the survey does not penetrate water. These regions were carefully analyzed to assess the reliability of the lidar data. A field survey was executed to validate the lidar data at several locations of interest. After generating a high-resolution (1×1 m) model bathymetry that encompasses the best available knowledge, a hydrodynamic model was developed and tested at a coarser grid resolution (10×10 m) that is practical for large-scale modeling. The test simulations used approximate initial and boundary conditions to investigate effects of different bathymetry processing options. This work sets the stage for more extensive model development.

This report is arranged as follows: Section 2 describes the procedures to process the lidar data (Task 1). Section 3 introduces the field survey and validation of the lidar data with the survey data (Task 2). Section 4 illustrates the selection, construction of the numerical model as well as the preliminary simulation results (Task 3). Section 5 summarizes the findings and discusses possible future improvements of the current study.

2 Lidar data processing

2.1 Creating a Digital Elevation Model (DEM) from lidar data

The two lidar datasets used in this project were obtained from Federal Emergency Management Agency (FEMA) surveys and processing: *FEMA2006*[1], which provides 1.4 m resolution raster data over the lower delta, and *FEMA2011*[2], which has approximately 1.0 m resolution for Liberty area. The coverage areas of these data are shown in Fig. 1, where the grid represents the available data subsets. The focus area for this study (yellow box in Fig. 1) encompasses 39 subsets from the *FEMA2006* dataset and 70 subsets from the *FEMA2011* dataset. For the *FEMA2006* dataset, each subset (corresponding to one data file) covers an area of about 4×5 km. These subsets were concatenated by matching the latitudes and longitudes at the boundaries. To meld the *FEMA2006* and *FEMA2011* datasets, a 1×1 m gridded mesh was defined over the study area. The *FEMA2006* data were interpolated onto this raster grid using the MATLAB *interp2* function. As the *FEMA2011* data points (given by latitude and longitude) were not uniformly distributed over space, the data from the 70 files were projected to the 1×1 m gridded mesh based on latitude and longitude bounding coordinates of each grid cell. Where multiple data points shared a single grid cell, the median of these points was used as the cell elevation. Where a cell had no data points, a NaN value was assigned. An area at the southern edge the study area is not available in the lidar coverage area and was assigned NaN values in the raster grid.

2.2 Noise removal and water body identification

A noise removal process is required before the rasterized lidar data can be used to generate the model bathymetry. Using one subset of the *FEMA2006* dataset as an example, the lidar data (interpolated to 1×1 m) can be found in Fig. 2, where three types of noise exists.

1. No data points (as represented by white blocks in Fig. 2).
2. Vertical stripes are found on large lakes, ponds and lagoons. These stripes are likely noise associated with the data collection flight path where the laser beam is reflected from the water surface.
3. Patchwork triangular blocks in some channels appear to be the remnant of interpolation methods (triangulated irregular network, TIN) applied in lidar data processing prior to data storage in *FEMA*. These features can be taken as an indication that few direct measurements were made in these channels.

Unfortunately, all the water areas in Fig. 2 (and throughout the Trinity data) typically belong to one of the three noise categories. Thus, there is no trustworthy information about the water depth within the *FEMA* data sets. However, the lidar data for the land seems

[1]FEMA, 2006, FEMA 2006 140cm Lidar, Texas Natural Resources Information System, `https://tnris.org/data-catalog/entry/fema-2006-140cm`

[2]FEMA, 2011, FEMA 2011 1m Parker Lidar, Texas Natural Resources Information System, `https://tnris.org/data-catalog/entry/fema-2011-1m-parker`

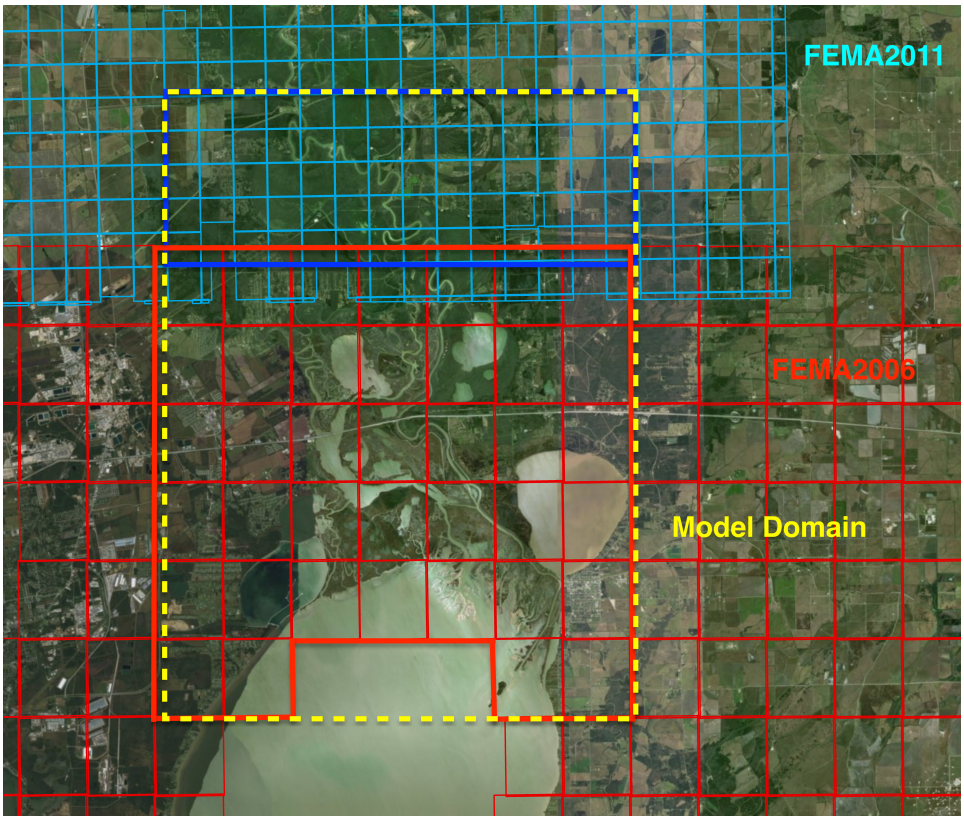

Figure 1: Scope of the lidar data. The red grids are the *FEMA2006* dataset. The blue grids are the *FEMA2011* dataset. The solid red and solid blue boxes are boundaries of data used in TDHM. The yellow box is the computation domain. (Source: Esri, DigitalGlobe, GeoEye, Earthstar Geographics, CNES/Airbus DS, USDA, USGS, AeroGRID, IGN, and the GIS User Community)

reliable (and has been spot-checked over limited extent, see Section 3). For further processing, the land regions and the water regions were separated within the dataset. To continue with the present model development without a comprehensive bathymetric survey, all water regions have been assigned a value of -1.0 m. This preserves connectivity of the channels visible at the lidar resolution, but likely misrepresents the actual water depth in many areas. If reliable bathymetric measurements for submerged regions can be provided in the future, the affected regions are easily identified and an algorithm to integrate the new data into the dataset can be developed.

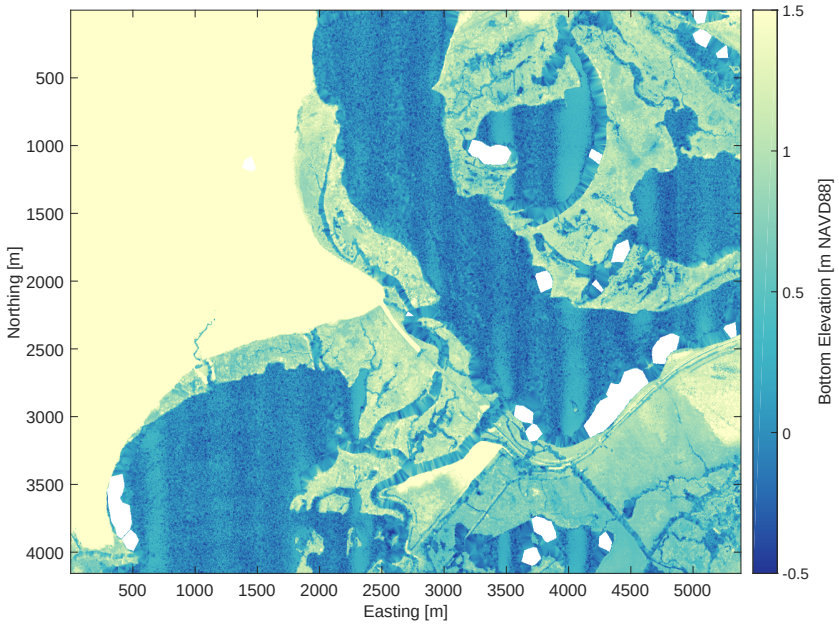

Figure 2: A subset of the raw lidar data from the *FEMA2006* dataset.

To separate the water regions from the land regions, the *kmeans* algorithm (e.g., Arthur & Vassilvitskii, 2007) was applied in conjunction with GoogleEarth satellite images. The *kmeans* approach is an image clustering algorithm commonly used in unsupervised machine learning. This approach uses an iterative process, grouping the pixels with similar properties (e.g., color) together until a cost function converges. More insights of this algorithm can be found in description of the function *kmeans* in the MATLAB Statistics and Machine Learning Toolbox. The present application of *kmeans* to discriminate between land and water requires the following workflow:

1. Obtain the GoogleEarth image that covers the region of the lidar data, called *imgA*.

2. Using the lidar data as a reference, correct the distortion in the satellite image by matching the scales of the objects in *imgA* and the lidar data. This task is accomplished

with the MATLAB functions *cpselect* and *fitgeotrans*. The result (for one data section) is Fig. 3, called *imgB*

3. Crop the distortion-fixed GoogleEarth image to get a portion of the image that matches the corresponding lidar data, called *imgC*. Selecting the regions to crop depends on the subjective judgement of the modeler, so some errors are expected.

4. Apply the *kmeans* algorithm on *imgC*. For the sample area shown the algorithm identifies 20 clusters from *imgC*. The resulting clustered map is shown as Fig. 4, called *imgD*.

5. The *imgD* pixels have values ranging from 1 to 20. Using *imgC* as a reference, the pixels indices that represent water areas are identified. In the example, it is clear that two shades of red colors and three shades of blue represent water. This step also depends on subjective judgement.

6. Finally, the water area pixels in the corresponding lidar data are replaced by a uniform bottom elevations (-1.0 m in this example), which provides the automatic (AU01) processed bathymetry at 1×1 m resolution, as Fig. 5.

As can be seen from Fig. 5, the majority of the water areas have been successfully identified. The wide channels and large lakes are sufficiently delineated. However, this method produced some extraneous water areas on the left of the figure that appear to be farmland or pasture. This approach also failed to identify some narrow channels. The main reason for these deficiencies is in the overall quality of the satellite image. The *kmeans* algorithm clusters the image based on colors, which must be separable in the satellite image. It is likely that the use of multiple satellite images taken at different times of the year (or in different years) could be used to improve this approach. Detailed review of the results show that at some locations the channels in the satellite image and the lidar data have horizontal location mismatches of up to 10 m. This occurs because (i) the distortion correction algorithms that match these datasets are approximations and do not create a precise overlay, and (ii) there can be transitional color features at the channel edges that affect the precision of its representation in the clustering algorithm.

The water-body identification procedure is applied for the entire study area to generate the high-resolution (1×1 m) bathymetry model, which is described in detail in Section 4.

Figure 3: GoogleEarth satellite image after distortion correction

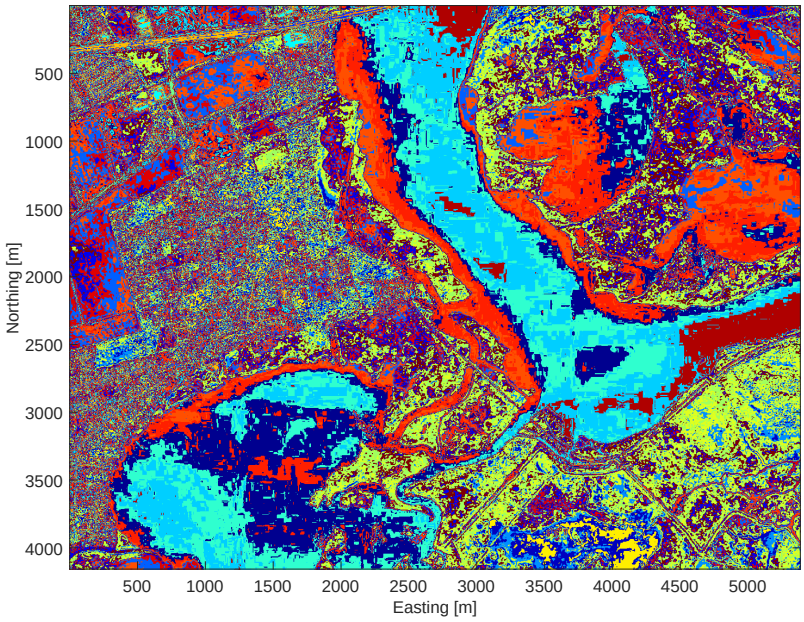

Figure 4: Clustered map of the distorting-corrected GoogleEarth image after cropping

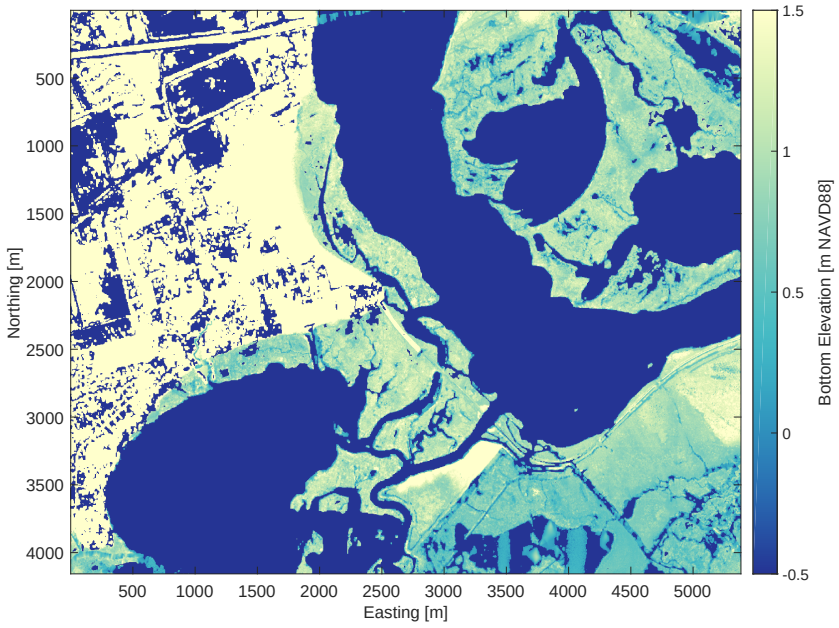

Figure 5: AU01 bathymetry created with automatic processing techniques from lidar data and clustered map.

3 Validation with field survey measurements

Although the clustering method successfully separated most of the land and the water regions, data for the water depth are lacking. A field trip organized by the Texas Water Development Board (TWDB) and the Trinity River Authority (TRA) was executed from Dec. 18th to Dec. 21st of 2016 to collect field data for validating the lidar data. The route of the field survey is shown in Fig. 6. Water depth is measured along main stream of the Trinity River as well as part of the Lost River. Several land elevations were also measured to examine the possible noise produced in the lidar data due to vegetation canopies. These field data are compared with the lidar data so that the reliability of the lidar data can be evaluated.

The surveyed water depths were converted into bottom elevations for the river channels. The survey depths have a mean of -3.296 m (NAVD88) and a median of -2.986 m, whereas none of the lidar data show deeper values than -0.5 m. Thus, the survey confirms that the *FEMA* dataset for submerged regions is not trustworthy.

To validate the land elevation, the median of the lidar data in a 50×50 m region (water areas excluded) centered at each of the land-validation locations (red dots in Fig. 6) were computed as a best estimate of the lidar land elevation. This value is compared with multiple field survey measurements that were taken at the same location. The absolute errors between the surveyed land elevations and the lidar results are shown in Fig. 7. Both the mean and the median of the absolute error are within 0.4 m, which provides a baseline for estimating uncertainty in the topography.

Figure 6: Route of the Trinity Delta field survey. The water depth was measured along the white path. The land elevation was measured at the red dots.

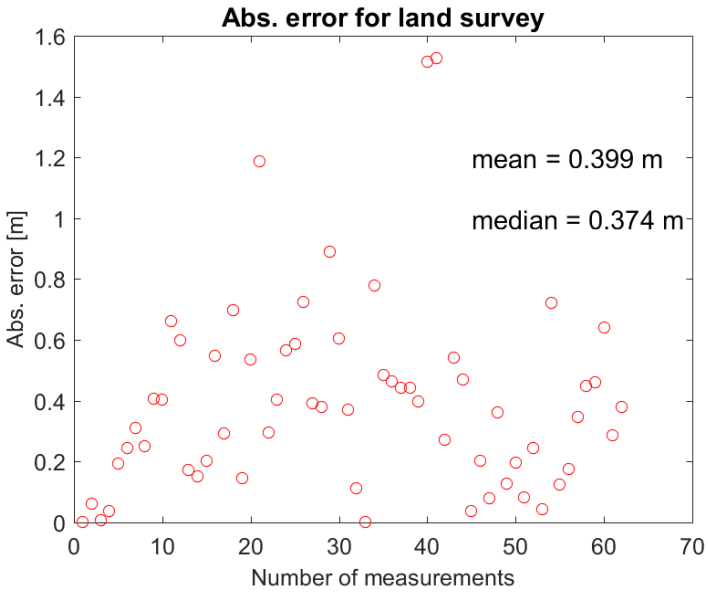

Figure 7: Absolute error of field surveyed land elevation and lidar data

4 Preliminary development of TDHM

4.1 Hydrodynamic model selection

The Frehd and SUNTANS hydrodynamic models were proposed as candidates for modeling of the Trinity Delta. The Frehd model is built on structured Cartesian grids, which are easy to use with the lidar dataset and has been successfully applied in a similar study in the Nueces River Delta (Ryan & Hodges, 2011). However, the Frehd model is computationally expensive for the larger Trinity Delta region as it is written as a set of MATLAB scripts. The SUNTANS model is compiled C code that is fast and parallelizes (Fringer, Gerritsen, & Street, 2006), but constructing the required high quality unstructured mesh with wetting and drying turned out to be laborious and time-consuming. The advantages of the two models were combined by rewriting the Frehd model in the C programming language and enabling parallel computing via the Message Passing Interface (MPI). In this way, the numerical model (referred as "Frehd-C") retains the ease-of-use of the original Frehd model at a significantly reduced computational cost.

Frehd-C solves the 2D depth-integrated free-surface Navier-Stokes equations with non-hydrostatic pressure and density gradients neglected. The solution algorithm is a hybrid finite-difference/finite-volume semi-implicit scheme that follows the methods originally designed by Casulli (Casulli & Cattani, 1994; Casulli & Cheng, 1992) with updates for turbulence modeling, accuracy, and stability (Hodges, 2015; Hodges, Imberger, Saggio, & Winters, 2000; Hodges & Rueda, 2008; Rueda, Sanmiguel-Rojas, & Hodges, 2007; Wadzuk & Hodges, 2009). The model is fundamentally mass conservative and allows the advective Courant-Friedrichs-Lewy (CFL) number to be slightly greater than unity in limited time/space areas without causing catastrophic instabilities. Furthermore, the barotropic CFL (associated with surface waves) can be significantly larger than unity across the entire domain while retaining a stable solution. When running in parallel mode, the computational domain is divided into equal subdomains by the number of computational threads. The subdomains communicate with each other by sharing the variables along their common boundaries. Ideally, linearly-increased speedup can be obtained with an increasing number of threads, but in practice the speedup is limited by overhead costs associated with a large number of threads. When executing with four threads, the Frehd-C code is approximately 10 times faster than the original Frehd. This speed-up is due to both the parallelization and the computational efficiency of a compiled C code compared to MATLAB. The Frehd-C was compiled on Mac Pro OSX El Capitan system (version 10.11.6) with Intel Xeon processor (64 GB memory).

Frehd-C models wetting and drying processes directly through the free surface solution, which follows the semi-implicit algorithm designed by Casulli and Cheng (1992). This approach allows dry cells to transition into wet cells based where the depth goes from zero to a positive value in the free-surface solution. To avoid both instabilities and the small time steps required for extremely small depths, a minimum depth threshold ($h_{min} = 10^{-3}$ m) is used. Where the local depth is below the threshold, a formerly wet cell is designated as a dry cell and the water surface elevation is set equal to the bottom bathymetry elevation. Dry cells remain in the computational domain but do not incur computational costs until

they become wet. To ensure scalar transport (e.g., salinity) remains conservative, Frehd-C limits the propagation of the wetting front in a single time step so that a newly-wet cell must be adjacent to an existing wet cell. As is typical of wetting/drying algorithms, the need to truncate very small depths and limit the wet front propagation speed leads to minor non-conservation of mass. This mass loss is tracked during the solution so that the user can be sure the solution is not degraded.

4.2 Modeling scenarios

The AU01 digital elevation model (Section 2) at 1×1 m resolution has 5.39×10^8 grid cells and would require a model time step of less than 0.1 seconds for stability. This scale of computation is not practical without use of high-performance supercomputers, which were not used in this study. For practical modeling on a desktop workstation the AU01 bathymetry was coarsened to 10×10 m by median filtering, which provides the AU10 digital elevation model that is shown in Fig. 8. This grid resolution has acceptable computational costs for short-period simulations (56 hours of wall-clock time for a one-day simulation using eight computational threads), but longer-term simulations on a desktop computer will likely require further coarsening of the grid. For example, a 20×20 m grid would have only 25% of the grid cells of the AU10 grid and allow a time step twice as long, which would require about 12.5% of the computational time of the AU10 grid. Thus, we expect that an AU20 bathymetry could be run at least 3× faster than real time. Similarly, an AU30 bathymetry should run approximately 12× faster than real time. Obtaining even faster run times would require either coarser bathymetric resolution or moving the computation to a supercomputer.

Although generating the AU10 bathymetry is straightforward and mostly automated, it introduces significant noise into the channel connectivity. The major channels are clearly identified but many secondary channels remain hidden. Thus, the AU10 bathymetry is unlikely to reproduce the correct surface connectivity needed to understand transport through the delta. To address this problem, a second bathymetry was created by using manual channel adjustments, resulting in the MA10 bathymetry shown in Fig. 9. The manual adjustments were made with Adobe Photoshop software using the GoogleEarth satellite images as a reference. The primary and secondary channels were delineated by hand on the AU10 data in Photoshop and the problematic noise features (discussed in Section 2.2) were removed. Unfortunately, this approach cannot (at this time) be reproduced with an automated method. Obtaining a more accurate bathymetric map with high-resolution channel connectivity remains a challenge in the absence of a complete on-the-ground survey of the channel depths.

The Frehd-C model requires initial conditions for the water depth throughout the domain and boundary conditions for the inflow and tidal boundaries. In addition, extensive field data is needed for model calibration and validation. Unfortunately, only the water level and flow rate data from a few USGS flow gages along the Trinity River and tidal elevations within Galveston Bay are available. In totality, these available data are inadequate for simulating, calibrating, and validating any specific real-world flow scenario. Thus, the Frehd-C model has been tested using idealized initial and boundary conditions to evaluate the capabilities

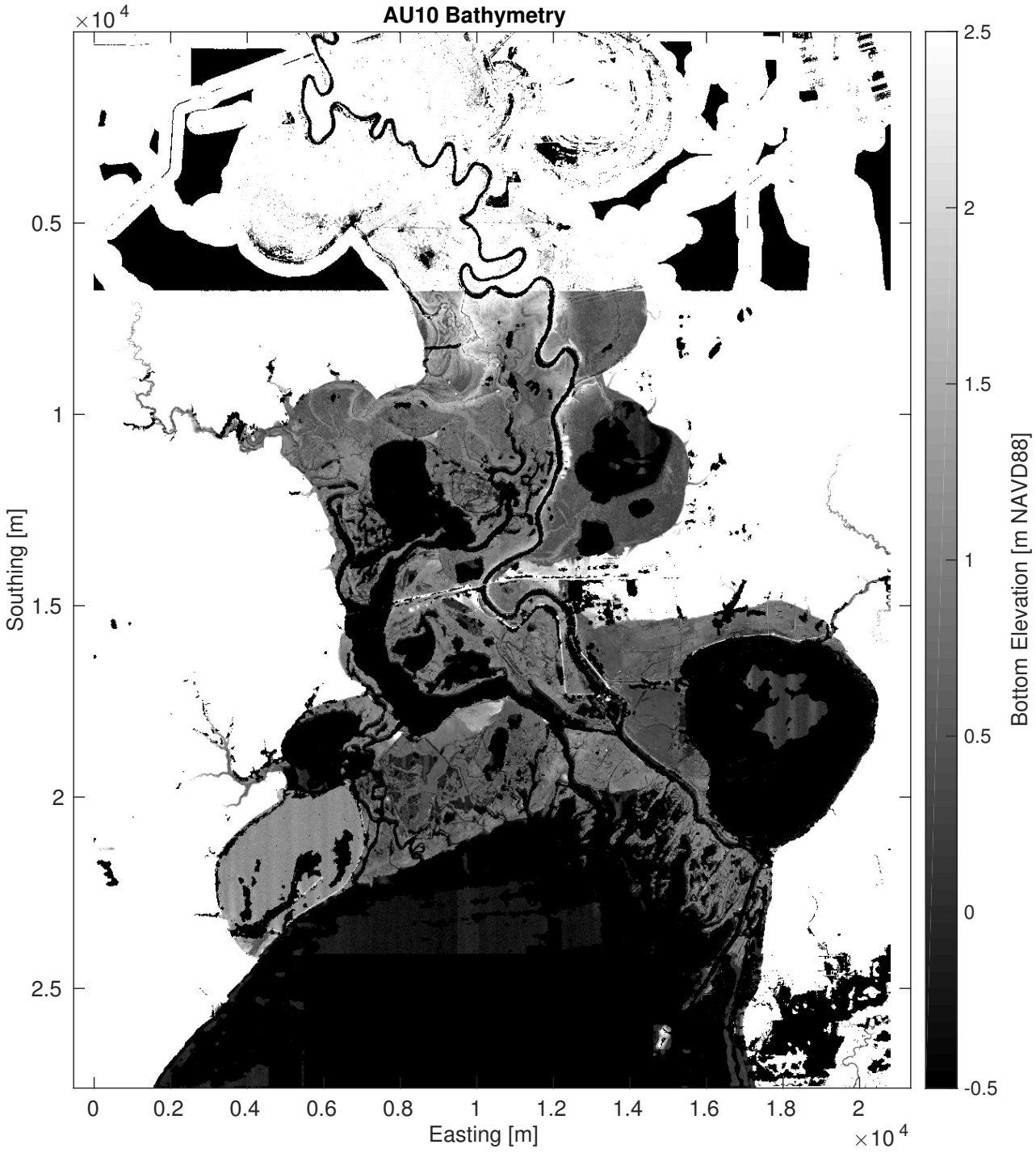

Figure 8: The AU10 bathymetry for the Trinity Delta created using the automatic clustering method. Black indicates water pixels where -1.0 m was assigned as the bottom elevation.

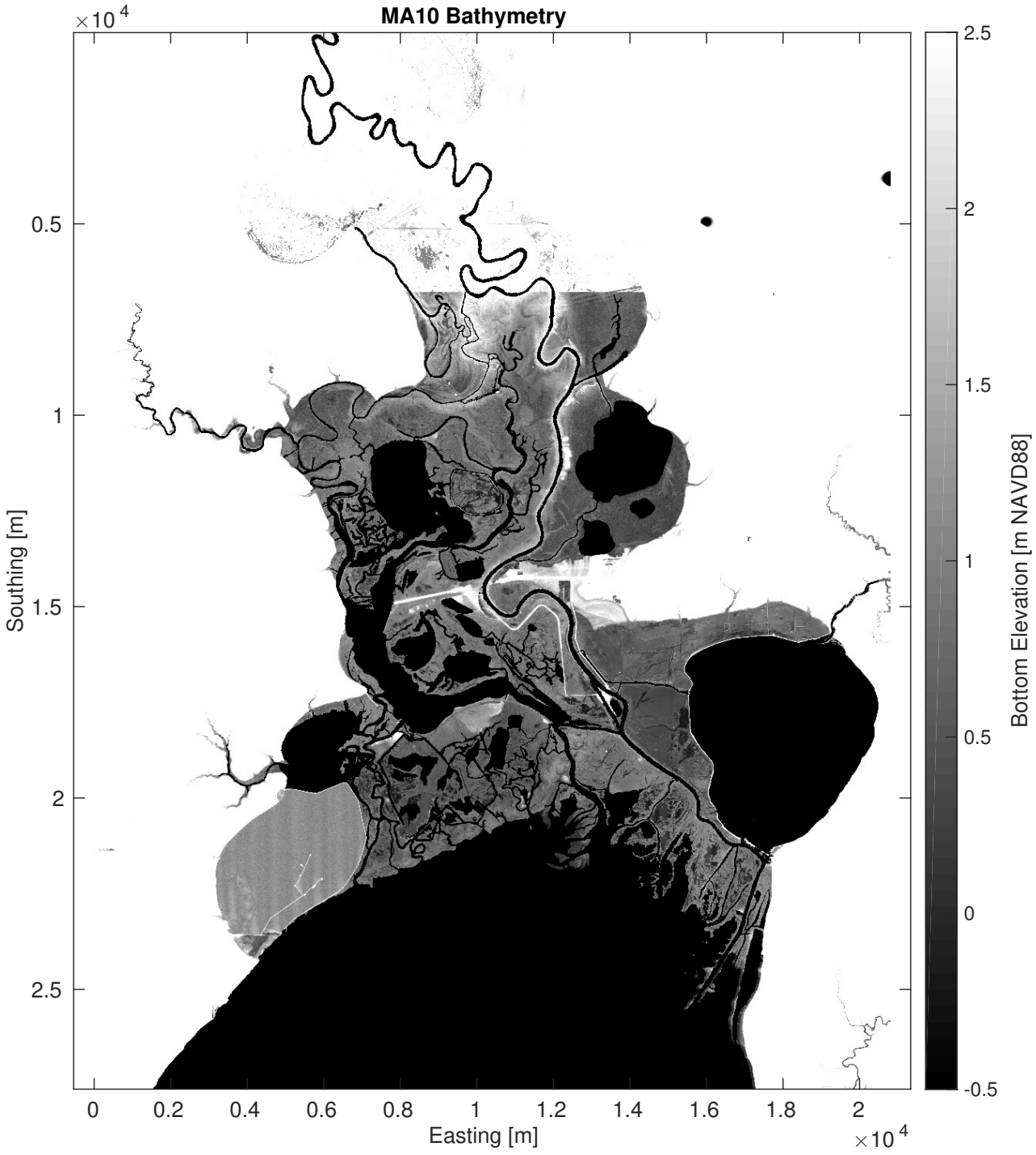

Figure 9: The MA10 bathymetry for the Trinity Delta created with manual adjustment for narrow channels. Black indicates water pixels where -1.0 m was assigned as the bottom elevation.

and limitations of the model with the AU10 and MA10 bathymetries.

Dirichlet boundary conditions (prescribed values for free-surface elevation) are used for both the south boundary in Trinity Bay and the north boundary of the Trinity River. The north boundary is defined using the water level measured at USGS 08067100, Trinity River near Moss Bluff (15 min sampling interval). The south boundary is defined as a sine wave representing an idealized tidal oscillation (Fig. 10). The model is initiated with a spatially-uniform free surface elevation ($\eta = 0$ m, NAVD88) and zero velocities. These test simulations are designed to examine the stability and efficiency of the model: investigating the physical details of the hydrodynamics and the transport processes is reserved for future studies. For simplicity and computational efficiency, the tested scenarios do not include a model spin-up period. Note that the initial surface matches the tidal boundary condition on the south but is discontinuous at the north boundary, which is a physically unrealistic initial condition. For practical future simulations, the initial surface elevation should be sloping to provide a continuous match to boundary conditions on both sides. Salinity is used as a passive scalar in the simulations to visualize net transport. Our modeling period is only one day (from Jan. 2nd to Jan. 3rd of 2017), which is much shorter than the residence time of the Trinity delta, so a spatially-varied salinity initial condition is set to help visualize short-term transport. The initial salinity field increases from north to south at an interval of 5 psu for every 3950 m. The salinity at the north boundary is 0 psu, while at the south boundary it is 40 psu. The wind speed and direction measured at USGS 08067252, Trinity River at Wallisville, are used to compute the wind stress (15 min sampling interval), which is assumed spatially-uniform across the model domain. During the modeling period, an east wind dominates with an average wind speed of 3.12 m/s. Other required model parameters for testing are listed in Table. 1.

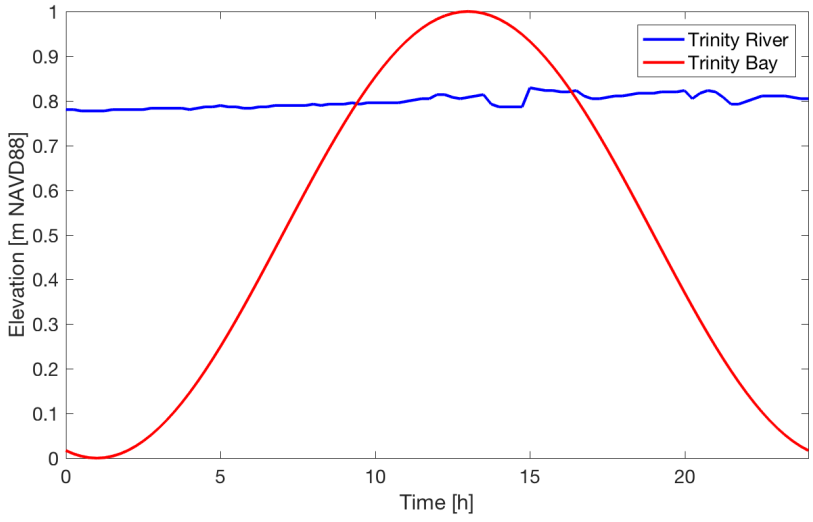

Figure 10: Boundary conditions at the south (Trinity Bay) and north (Trinity River) edges of the simulation domain

Parameter	Value	Description
Δt [s]	1	time step
Δx [m]	10	grid size
Δy [m]	10	grid size
ν [$m^2 s^{-1}$]	0.0001	eddy viscosity
C_D	0.01	bottom drag coefficient
h_D [m]	0.001	minimum depth allowed
N_p	6	number of threads

Table 1: Frehd-C model parameters for idealized tests

4.3 Model results

Figure 11 shows the modeled free surface elevation for the MA10 bathymetry at four selected times. Figure 12 shows the similar modeled free-surface elevation for the AU10 bathymetry that was generated by an automatic process without manual interference. In comparing these results, it can be seen that the AU10 tends to build up higher water surface elevations in the lower-to-middle delta. Arguably, this is because the lack of connectivity of the small channel network in the AU10 bathymetry for the middle-to-upper delta. These small channels are effectively the relief valve that allows water from the lower delta to be pushed inland, and lack of these paths in the AU10 bathymetry causes the water to accumulate in the lower delta. These results indicate the overall importance of the small channels in the flow physics. Despite their small size, they have a visible effect on the inundation patterns.

Figure 13 shows the modeled salinity using the MA10 bathymetry. Tidally-driven transport into the Trinity Delta is clearly observed. The lower part of the delta experiences relatively significant dispersion and mixing. In the upper part of the delta, the salinity field varied more slowly. Freshwater in the upstream river pushes both downstream and into the delta through upstream channels.

Figure 14 shows the modeled salinity for the AU10 simulation. A major difference between the MA10 and AU10 simulations is the downstream extent of freshwater, which is significantly further in the AU10 bathymetry. This result is consistent with the surface elevation results, where the lack of connectivity to small channels in the upper delta allows higher water elevations in the main river channel upstream, which leads to a more significant surface gradient that drives freshwater further downstream in the main channel. However, it is difficult to draw conclusions from these comparisons as a non-conservation warning for scalar concentrations was produced in the simulation with AU10 bathymetry. The precise reason for conservation failure is not yet known, but is likely due to incompatibility between the Frehd scalar limiter and the MPI algorithm, which requires further investigation.

These preliminary model results indicate that the different bathymetry processing techniques have a significant impact on transport within the delta. Specifically, the complex narrow channel network in the mid-to-upper delta receives and stores a significant volume of water, and neglecting these volumes can lead to overpredicted surface water elevation in the lower delta. Correctly representing both the surface connectivities and overall volumes of these channels is thus important and is a challenge to the lidar data processing techniques and the coarsening of the bathymetry to produce a computationally-practical model.

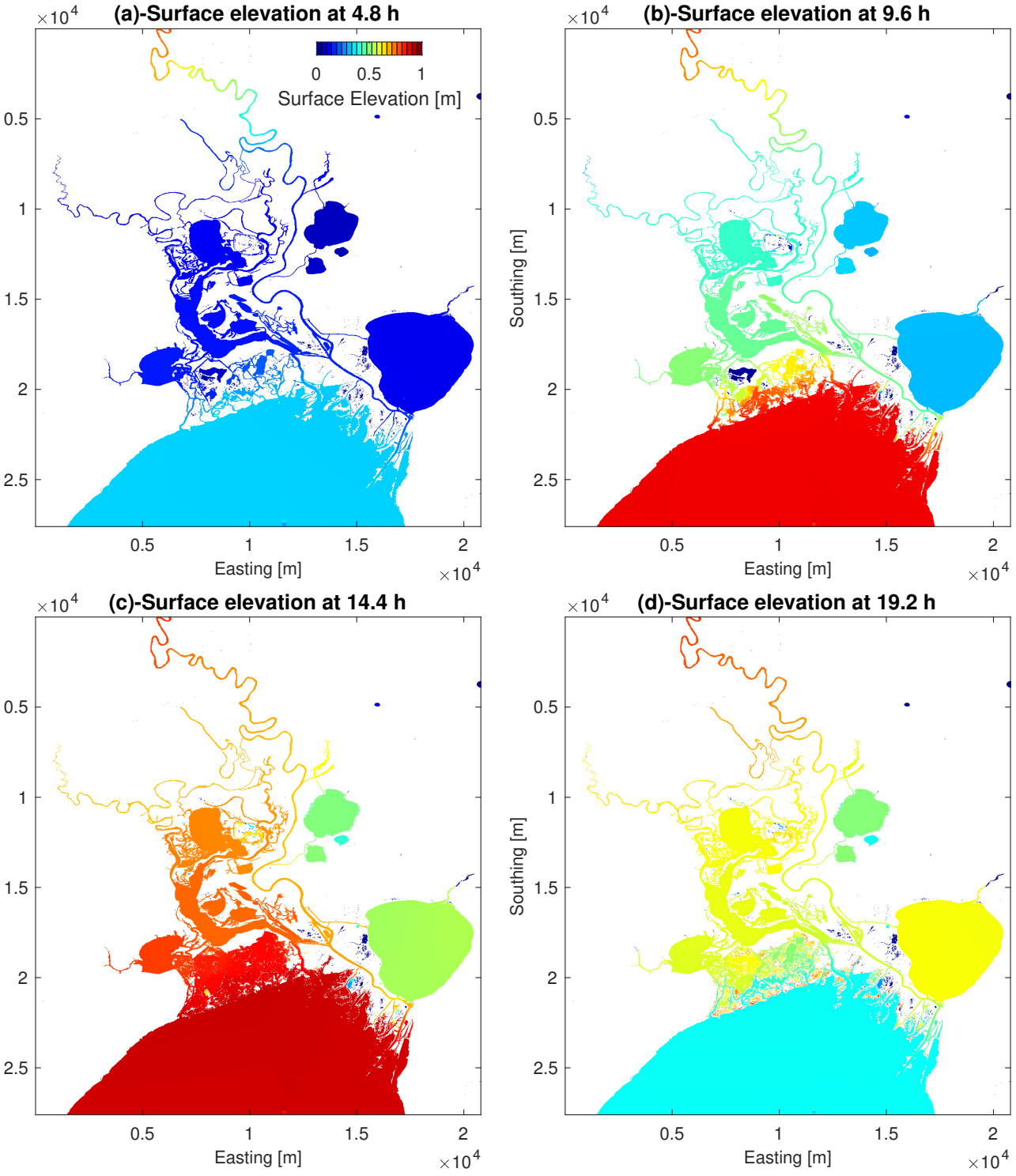

Figure 11: Modeled surface elevation for the MA10 bathymetry at 4.8, 9.6, 14.4 and 19.2 hours after model starts, which corresponds to 20%, 40%, 60% and 80% of the total simulation time.

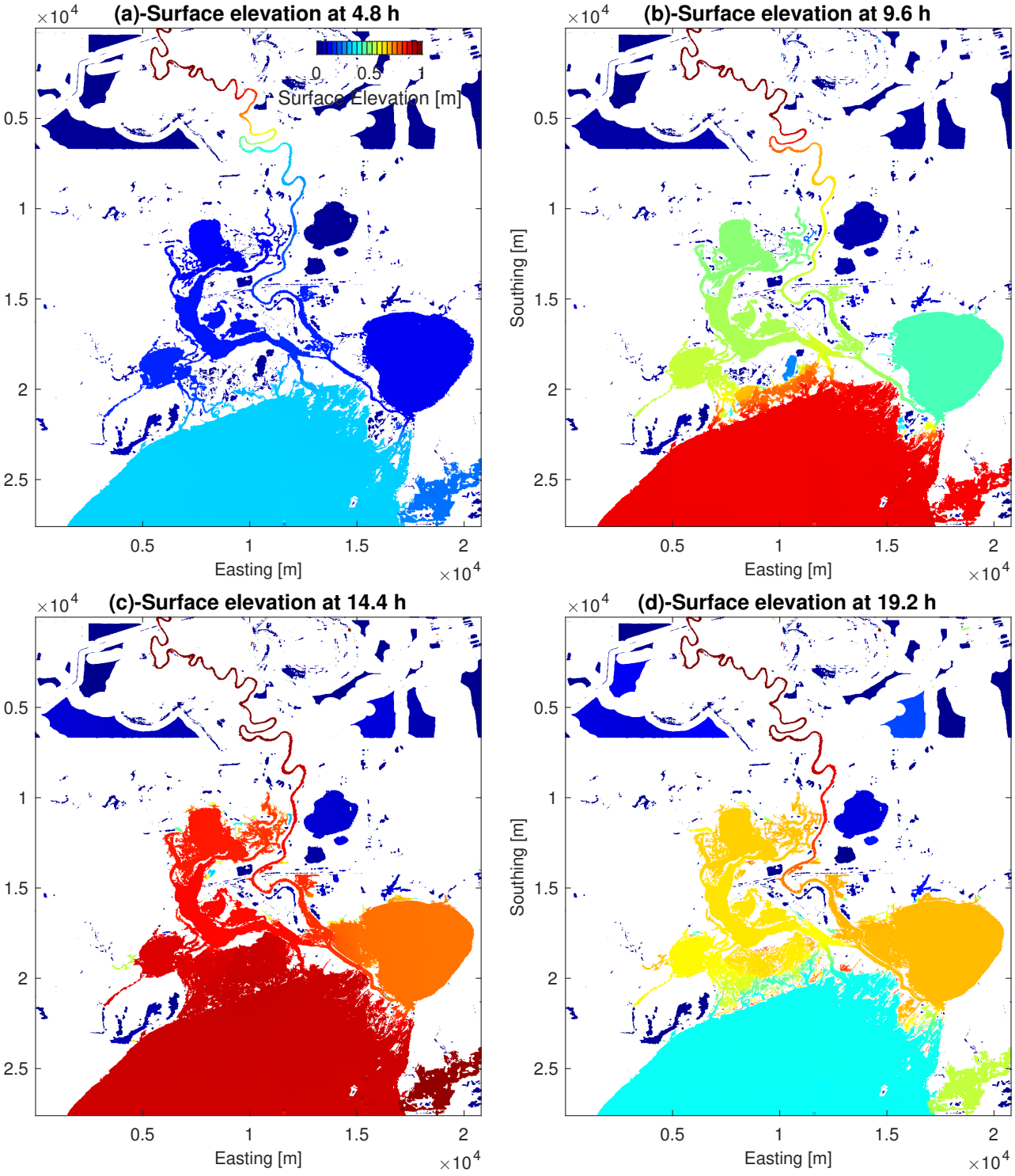

Figure 12: Modeled surface elevation for the AU10 bathymetry at 4.8, 9.6, 14.4 and 19.2 hours after model starts, which corresponds to 20%, 40%, 60% and 80% of the total simulation time.

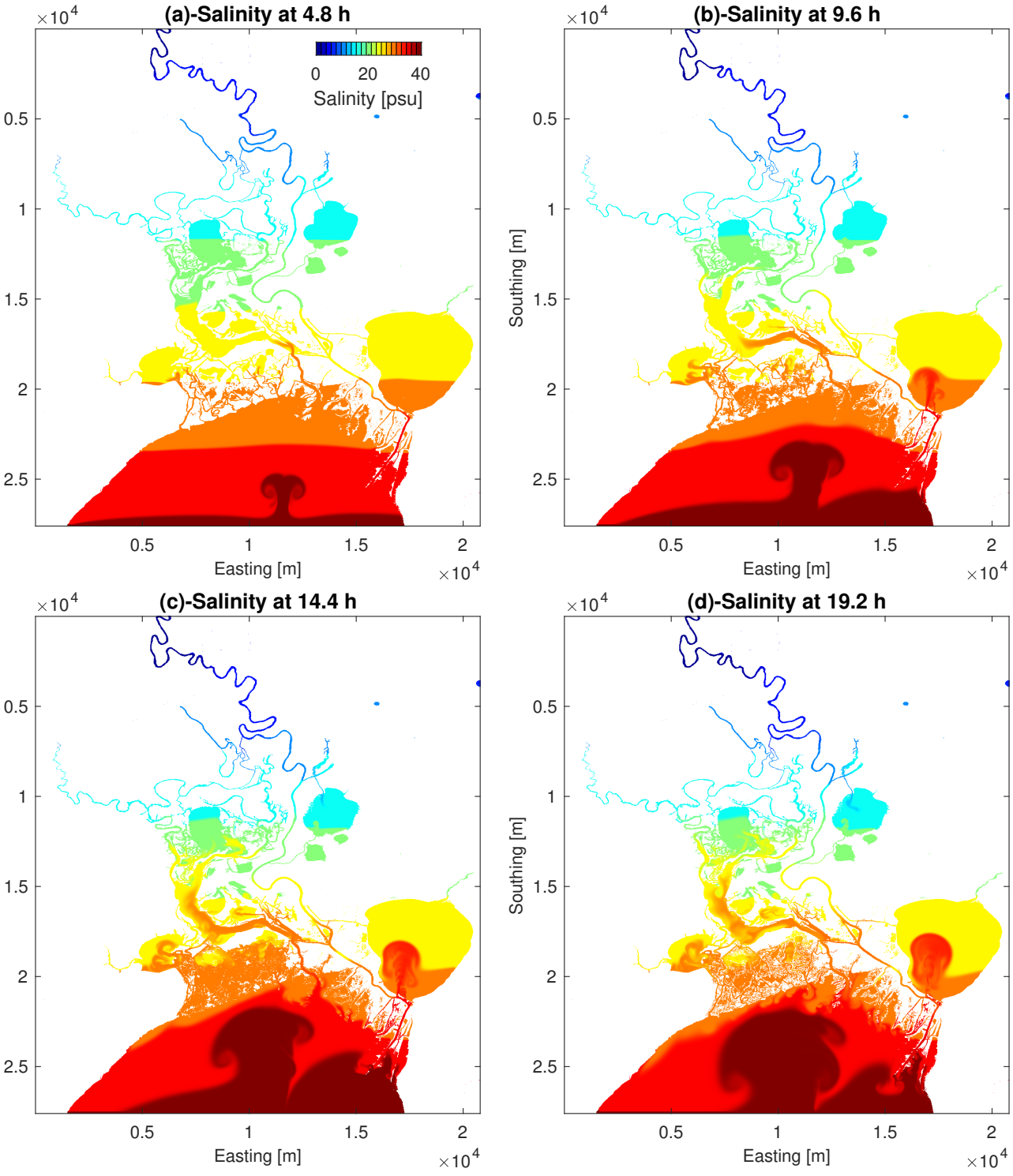

Figure 13: Modeled salinity for the MA10 bathymetry at 4.8, 9.6, 14.4 and 19.2 hours after model starts.

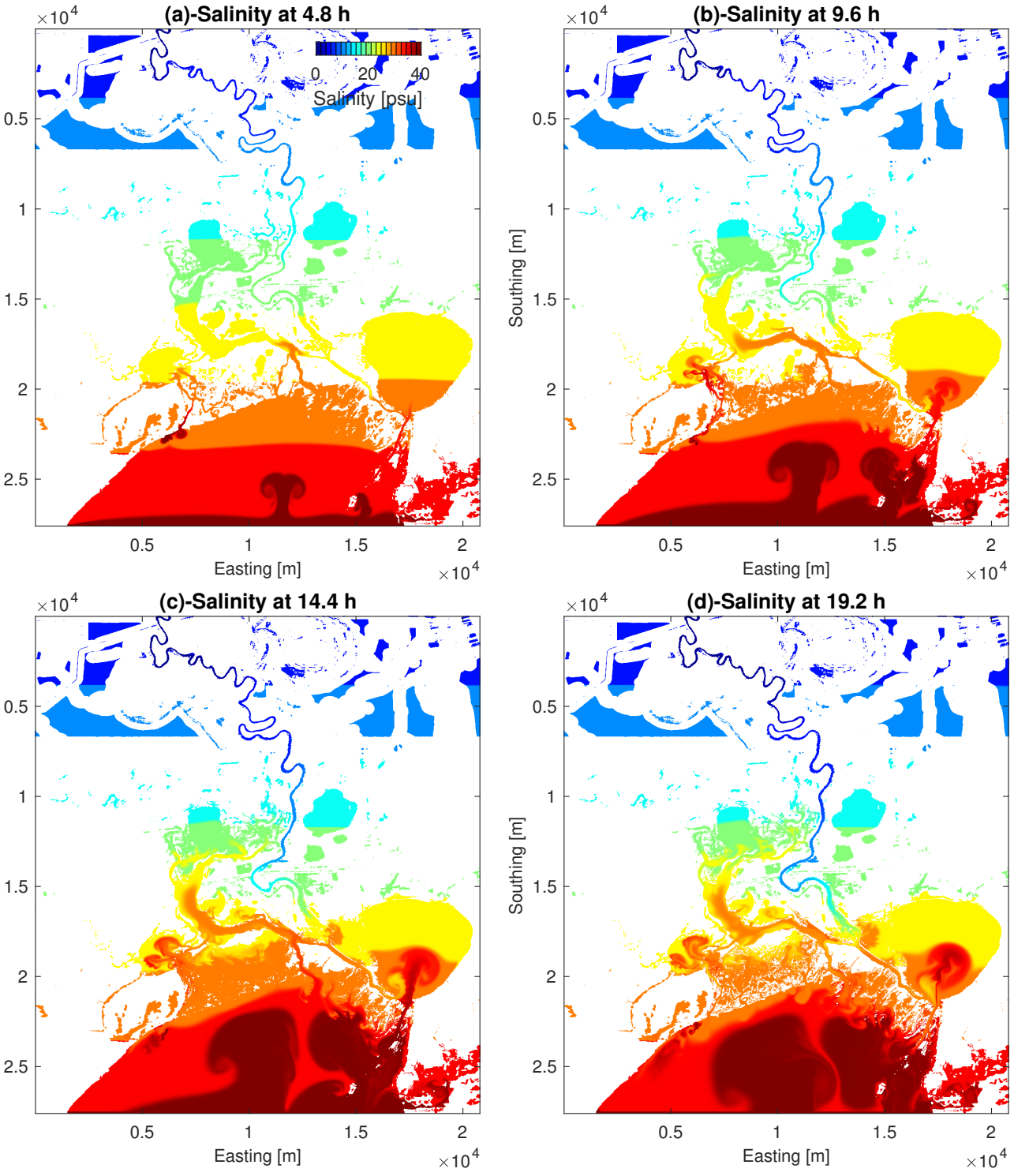

Figure 14: Modeled salinity for the AU10 bathymetry at 4.8, 9.6, 14.4 and 19.2 hours after model starts.

5 Summary and future tasks

This project developed a bathymetric model for the Trinity Delta using the best-available data at 1×1 m resolution. A hydrodynamic model of the delta at 10×10 m grid resolution has been developed and tested. Preliminary results show that the bathymetric representation of small-channel connectivity and volume in the middle-to-upper delta may significantly influence the simulated water surface elevations and transport in the delta. Correctly representing these channels in the model remains a challenge because (i) the model runs on a 10×10 m grid, which overestimates some channels and cannot represent others, and (ii) the *FEMA* lidar datasets do not include reliable bathymetry in any of the submerged areas, including the small channels. Methods to better represent the effects of small channels at coarse grid scales are presently being developed.

Translating lidar topography into an adequate model bathymetry for a river delta is a complex task that requires judgement of the analyst and some manual adjustments. Automated approaches that assist in this effort and reduce the amount of manual processing have been developed herein, but as yet these cannot be entirely relied on to discriminate between submerged and unsubmerged topography in the *FEMA* lidar data. A key roadblock to automated analyses is the quality of the satellite photographs used for image discrimination. It is likely that higher quality and/or multi-spectrum images could be effectively used for improving the processing. However, no amount of processing can overcome the lack of adequate data in the submerged portions of the system.

Extending the present model to represent a particular simulation period will require more extensive data for calibration, validation, and boundary conditions. The prior TWDB deployment of CTD (conductivity, temperature and depth) sensors across wide swaths of the Nueces River Delta (Schoenbaechler, Negusse, & Guthrie, 2014) is a prototype for the type of deployment needed in the Trinity Delta. However, it should be noted that fluxes of near-surface groundwater across the Trinity Delta are likely to affect the total water storage, residence time, and surface-water flows through the system. The Frehd-C model does not presently include groundwater storage/flux computations, although this feature could be readily added. More challenging than adding the groundwater fluxes to the model is the effort required for collecting adequate data to calibrate and validate groundwater effects.

References

Arthur, D., & Vassilvitskii, S. (2007). K-means++: The advantage of careful seeding. In *Soda 07: Proceedings of the eighteenth annual acm-siam symposium on discrete algorithms* (pp. 1027–1035).

Casulli, V., & Cattani, E. (1994). Stability, accuracy and efficiency of a semi-implicit method for three-dimensional shallow water flow. *Comput. Math. Appl.*, *27*, 99 112.

Casulli, V., & Cheng, R. T. (1992). Semi-implicit finite difference methods for three-dimensional shallow water flow. *International Journal for Numerical Methods in Fluids*, *15*, 629–648.

Fringer, O. B., Gerritsen, M., & Street, R. L. (2006). An unstructured-grid, finite-volume, nonhydrostatic, parallel coastal ocean simulator. *Ocean Modelling*, *14*, 139–173.

Hodges, B. R. (2015). Representing hydrodynamically important blocking features in coastal or riverine lidar topography. *Natural Hazards & Earth System Sciences*, *56*, 1011–1023.

Hodges, B. R., Imberger, J., Saggio, A., & Winters, K. (2000). Modeling basin-scale internal waves in a stratified lake. *Limnology and Oceanography*, *47*(7), 1603–1620.

Hodges, B. R., & Rueda, F. J. (2008). Semi-implicit two-level predictor-corrector methods for non-linearly coupled, hydrostatic, barotropic/baroclinic flows. *International Journal of Computational Fluid Dynamics*, *22*(9), 593–607.

Rueda, F. J., Sanmiguel-Rojas, E., & Hodges, B. R. (2007). Baroclinic stability for a family of two-level, semi-implicit numerical methods for the 3D shallow water equations. *International Journal of Numerical Methods in Fluids*, *54*(3), 237–268.

Ryan, A. J., & Hodges, B. R. (2011). *Modeling hydrodynamic fluxes in the Nueces River Delta* (Tech. Rep.). Center for Research in Water Resources, University of Texas at Austin. (CRWR Online Report 11-07, 92 pages, October 2011)

Schoenbaechler, C. A., Negusse, S., & Guthrie, C. G. (2014). *Nueces delta data collection for calibration and validation of the nueces delta hydrodynamic model* (Tech. Rep.). (Final Report to the U.S. Army Corps of Engineers, Fort Worth District. January 21, 2014. Texas Water Development Board. Austin, TX. 46 pp)

Wadzuk, B. M., & Hodges, B. R. (2009). Hydrostatic versus nonhydrostatic Euler-equation modeling of nonlinear internal waves. *ASCE Journal of Engineering Mechanics*, *135*(4), 1069–1080.